



A water-soluble polysaccharide from *Eucommia folium*: the structural characterization and anti-tumor activity *in vivo*

Zhi-Qian Yan¹ · Su-Yun Ding¹ · Pei Chen¹ · Hui-Ping Liu¹ · Meng-Li Chang¹ · Shu-Yuan Shi¹

Received: 30 May 2022 / Revised: 8 October 2022 / Accepted: 11 October 2022 / Published online: 7 November 2022
© The Author(s), under exclusive licence to Springer Science+Business Media, LLC, part of Springer Nature 2022

Abstract

In this study, a water-soluble polysaccharide from *Eucommia folium* was extracted by hot water and purified using Sephadex G-200 gel columns. The results showed that the purified fraction (EFP) has a molecular weight of 9.98×10^5 Da and consisted of rhamnose, arabinose, galactose, glucose, mannose, xylose, galacturonic acid, and glucuronic acid (molar ratio: 0.226: 1.739: 2.183: 1: 0.155: 0.321: 0.358: 0.047). The combination of infrared spectroscopy and NMR analysis proved that EFP is an acidic polysaccharide whose main chain consists of α -L-Araf-(1 \rightarrow , \rightarrow 3,5)- α -Araf-(1 \rightarrow , \rightarrow 3)- β -Galp-(1 \rightarrow , \rightarrow 3,6)- β -GlcP-(1 \rightarrow , \rightarrow 2)- α -D-Manp-(1 \rightarrow , \rightarrow 4)- α -GalpA-(1 \rightarrow , \rightarrow 2,4)- α -Rhap-(1 \rightarrow). In addition, the *in vivo* antitumoral activity of EFP was studied using a H22 tumor-bearing mice model. EFP effectively inhibited tumor growth in mice following intragastric administration. By Combining with the results of the apoptosis assay and JC-1 staining analysis, we confirmed that EFP induces apoptosis through the mitochondrial pathway. Furthermore, cell cycle analysis demonstrated that EFP blocks the cell cycle at S phase.

Keywords *Eucommia folium* polysaccharide · Structure characterization · Antitumor activity · Human hepatocellular carcinoma

Introduction

Liver cancer is still a major threat to human health [1]. Its incidence rate is as high as 70–90% [2], and its mortality rate is behind gastric and esophageal cancer [3]. The most common liver cancer is hepatocellular carcinoma (HCC). Its early symptoms are difficult to detect, and many patients are already at an advanced stage when diagnosed [4]. Currently, the most general treatment methods are mainly surgical resection, chemotherapy and radiotherapy. However, due to the significant toxicity associated with chemotherapy and radiotherapy, the patients' life expectancy is markedly shortened [5, 6]. Although first-line drugs such as sorafenib, cisplatin and 5-Fluorouracil (5-Fu) show certain therapeutic effects, clinical studies have found that these drugs are associated with drug resistance, cytotoxicity,

and immunosuppression [7, 8]. In spite of the progress that has been made in many areas, particularly in determining the most common causes of HCC and improving diagnostic tools, the complexity of liver cancer treatment remains daunting [9]. Therefore, traditional Chinese medicine has attracted much attention in cancer treatment. Compared with traditional antineoplastic drugs, traditional Chinese medicines and their components usually have many advantages with minimal side effects [10]. These advantages might be a crucial research orientation for future cancer treatments.

Macromolecular carbohydrates are composed of more than ten monosaccharides, known as polysaccharides. Previous research on polysaccharides identified large amounts of polysaccharides from multiple sources, such as mushrooms, bacteria, animals, and plants [11–13]. These polysaccharides have aroused much attention for their extensive bioactivities and low cytotoxicity [14]. At least 30 polysaccharides have been used in clinical trials around the worldwide [15]. Recently, many studies found that polysaccharides can induce tumor cell death, enhance the body's immune capacity, diminish the toxic effects of traditional chemotherapy medicines, and achieve the purpose of antitumoral effects [16, 17].

✉ Hui-Ping Liu
liuhuiping111@163.com

¹ State Key Laboratory of Food Nutrition and Safety, Key Laboratory of Food Nutrition and Safety, Ministry of Education of China, College of Food Science and Engineering, Tianjin University of Science & Technology, Tianjin 300457, People's Republic of China

Eucommia ulmoides is a medicinal plant that can be traced back to the Shennong Baicao Records dating 2000 years ago. Traditionally, the bark of *Eucommia ulmoides* was used as medicine [18], and it was often used as a tonic to keep fit and nourish liver in ancient Chinese medicine books [19]. The same active ingredients and pharmacological effects have been found in both *Eucommia folium* and the bark of *Eucommia ulmoides* [20, 21], including iridoids, flavonoids, lignans and polysaccharides. Studies have found that *Eucommia folium* has antihypertension, anti-inflammatory, antioxidant, antifatigue and obesity-preventive effects [22]. In addition, *Eucommia ulmoides* polysaccharides have been demonstrated to enhance immune activity, and adjust macrophages-mediated immunity, leading to anti-inflammatory effects [23]. The literature about *Eucommia folium* polysaccharide and its antitumor activity is rare, and therefore, in this study, we investigated structure and antitumor activity of EFP. We prepared the acidic polysaccharide (EFP) through hot water abstraction and alcohol precipitation. Furthermore, we inoculated mice with H22 hepatocellular carcinoma cells to investigate the in vivo antitumor capacity of EFP and explore its potential mechanism in inducing tumor cells apoptosis.

Materials and methods

Materials

Eucommia folium was acquired from residents in Dabie Mountain (Anhui, China). Monosaccharide standards, T-series dextran standards and 5-fluorouracil were all purchased from Sigma, USA. Sephadex G-200 was bought from Shanghai Yuanye Biological Technology Co.,Ltd. The JC-1 mitochondrial membrane potential detection kit was obtained from Beijing Solarbio Science & Technology Co.,Ltd. The Annexin V-FITC/PI apoptosis detection kit was purchased from Dalian Meilun Biotechnology Co.,Ltd. The cell cycle and apoptosis kits were obtained from Beyotime Biotech (Jiangsu, China). All other chemical reagents and materials were of analytical grade.

Cells and cell culture

H22 hepatocarcinoma cells were provided by Tianjin Solomen Biotechnology Co.,Ltd. The cells were cultured in medium supplemented with 10% fetal bovine serum, 100 U/mL penicillin and 100 µg/mL streptomycin.

Extraction and purification of EFP

The *Eucommia folium* was desiccated in drying oven at 50 °C until constant weight. Then the dried *Eucommia*

folium was crushed over the 60-mesh sieve. The obtained powder (10 g) was boiled three times in distilled water (200 mL) for 3 h each time. The aqueous extract was centrifuged at 4000 rpm at 25 °C for 15 min, and the supernatant condensed to one-third volume using a rotary evaporator, and then precipitated with 60% (v/v) absolute ethanol at 4 °C for 12 h. The crude polysaccharide was acquired through centrifugation (4000 r/min, 10 min).

The crude polysaccharide solution was prepared with distilled water and the insoluble impurities removed by centrifugation (8000 r/min, 10 min). The supernatant was used to remove proteins by the Sevag method [24], and the organic reagent was removed using the rotary evaporator. The polysaccharide solution was dialyzed with 100 kDa dialysis tubes in 4 °C distilled water for 3 days and then freeze-dried. The obtained polysaccharides were eluted through a Sephadex G-200 (1.6 × 40.0 cm) gel column at the elution condition of 0.1 mL/min, and collected for 15 min in each tube. The components in each eluent tube were tested by the phenol–sulfuric acid method. The eluent was collected, and freeze-dried, and high-purity polysaccharides were obtained and named EFP for further research.

Structural characterization of EFP

Chemical composition detection and UV spectroscopy

By taking D-glucose as standard, the EFP total sugar content was determined by the phenol–sulfuric acid method [25]. The protein content of EFP was detected with BSA as standard using the Coomassie brilliant blue method [26]. Using galacturonic acid as standard, the EFP content in uronic acid was examined by the sulfuric acid-carbazole method [27]. A 1 mg/mL EFP solution was prepared for testing, while distilled water was used as blank control, and UV spectrum analysis was performed in the range of 200–900 nm.

Detection of molecular weight distribution

High performance gel-permeation chromatography (HPGPC) (Agilent-1200) using a TSK-Gel G4000PWxl column was used to examine EFP molecular weight. The differential refractive index detector (RID) was selected using a temperature detector at 35 °C. The other test conditions were as follows: the column temperature was set as 30 °C, the sample volume was 20 µL (1 mg/mL), and the flow rate of 0.6 mL/min was eluted with ultrapure water as a mobile phase. The standard curve of dextran T-10, T-40, T-70, T-110, T-500, and T-2000, with known molecular weight,

was established, and EFP molecular weight was calculated based on the standard curve [28].

Ion chromatography assay

Ion chromatography (IC) was employed to detect EFP monosaccharide composition. EFP (5 mg) and 1 mL 2 M trifluoroacetic acid (TFA) were fully mixed and hydrolyzed at 110 °C for 3 h. The TFA was removed by Termovap Sample Concentrator, and 1 mL methanol was added to the sample and dried with nitrogen. These steps were repeated three times to ensure that the TFA was completely removed. Acid hydrolysate was completely dissolved in 1 mL ultrapure water and the concentration was adjusted to 150 ppm for IC analysis. Meanwhile, D-glucose, D-galactose, D-fucose, L-rhamnose, D-xylose, D-mannose, L-arabinose, D-glucuronic acid and D-galacturonic acid mixtures with the concentration of 50 ppm were prepared for testing on IC. The Dionex ISC5000 chromatographic system (CA, USA) was used with the high efficiency anion exchange column of Dionex CarboPac PA10 (150 mm × 3 mm) and Dionex pulsed current detector. The column temperature was 30 °C. A solution combining 10 mM NaOH and sodium 200 mM acetate were used as mobile phases. The flow rate of 0.5 mL/min was used for gradient elution.

FT-IR assay and NMR of EFP

Totals of 1 mg EFP and 150 mg KBr were mixed and ground into a thin slice. The Fourier transform infrared spectrophotometer (Bruker Vector-22, Karlsruhe, Germany) was used to determine the infrared spectrum of EFP in the wavelength range of 4000–400 cm^{-1} [29].

A total of 60 mg EFP was fully dissolved in 0.5 mL D_2O . The Bruker Advance DPX-500 MHz spectrometer was used to obtain the ^1H , ^{13}C , COSY and HSQC NMR spectra of EFP [30].

SEM observation

The small amount of dry sample was affixed to the conductive adhesive surface fixed on sample table to ensure its uniform thickness. After sputtering with gold, the EFP surface structure and morphology were observed by SEM (SU1510, Japan) at 1000 ×, 2000 × and 3500 × magnification, respectively.

Congo red assay

Congo red analysis is a method commonly used to detect the triple helix conformation of polysaccharides [31]. The EFP solution (2 mL, 0.5 mg/mL), the Congo red solution (2 mL, 50 μM) and the NaOH (1 M) solution were mixed to obtain final concentrations of 0, 0.05, 0.1, 0.15, 0.2, 0.25, 0.3, 0.35,

0.4 mol/L. Meanwhile, the mixed solution without EFP was used as control. After 15 min of reaction at room temperature, an ultraviolet spectrophotometer was used to detect the maximum absorption wavelength of the solution within 400–600 nm.

EFP in vivo antitumor activity

Establishment of H22 tumor-bearing mice model

Fifty Kunming SPF female mice (6–8 weeks old, weight 20 ± 2 g) were obtained from Sibeifu Experimental Animal Co., Ltd (Beijing). They were fed in the Experimental Animal Center of Tianjin University of Science and Technology. They were kept in an indoor relative humidity at 45%–55% and a temperature of 22 ± 2 °C. During the experiment, the mice were provided water and food, and 12-h light and dark cycle. The animal experiments were conducted in accordance with the Regulations on the Administration of Laboratory Animals [32]. After 1 week of acclimation, 50 mice were randomly assigned into the following five groups (10 mice in each group): blank group, model group (negative control), 5-fluorouracil group (5-Fu group, positive control), 100 mg/kg EFP group and 300 mg/kg EFP group. Apart from the blank group, the other mice were inoculated with 0.2 mL H22 cells' suspension (cell density: 1×10^6 cells/mL) under the right forearm. The model and the blank groups were given 0.2 mL saline every day, the 5-Fu group was injected with 0.2 mL of 5-Fu (20 mg/kg), and the low-dose and high-dose groups were intragastrically administered with 0.2 mL (100 mg/kg, 300 mg/kg) of EFP. The treatments lasted up to three weeks, and the mice weight was measured once a week. The hair and behavior characteristics of the mice were observed.

Solid tumor and immune organ index in mice

Four weeks into the experiment, the mice were sacrificed using the neck breaking method. The mice solid tumors, thymus, and spleen were dissected. The blood stains were washed with saline and the solution was absorbed with filter paper and the tissues were accurately weighed. Tumor length (L, cm) and width (W, cm) were measured with a vernier caliper, and the tumors' volume was obtained using the following formula: $V(\text{cm}^3) = \frac{LW^2}{2}$. The tumor inhibition rate (%) was calculated by the following equation: $\text{tumor inhibition rate}(\%) = \frac{G_1 - G_2}{G_1} \times 100$. G_1 represented the average tumor weight of the model group, G_2 represented the average tumor weight of each therapeutic group. The immune organ index was computed by the formula:

$$\text{immune organ index} = \frac{\text{the average weight of the immune organs}}{\text{the average body weight of the mice}}$$

Histological analysis

Tissue blocks of soy-sized were cut from tumor and liver tissues, fixed with 4% paraformaldehyde for 24 h, embedded with paraffin, and sliced into 5 μm sections. All tissue sections were stained according to the standard method in the hematoxylin and eosin (H&E) kit, and then observed under the microscope.

Apoptosis analysis

The tumor tissues of appropriate size were cut and gently grounded on 200-mesh cell screen, then repeatedly rinsed with saline. The abrasive solution was centrifuged at 1000 rpm for 5 min. The tumor cells were resuspended with PBS and the concentration adjusted to 1×10^6 cells/mL. Subsequently, the Annexin V-FITC/PI kit was utilized to measure cell apoptosis. Cell precipitates were collected by centrifugation, resuspended with 100 μL 1 \times Binding Buffer, and then the Annexin V-FITC (5 μL) and PI (5 μL) staining solutions were added. After 10 min incubation at 25 $^\circ\text{C}$ under dark condition, 500 μL 1 \times Binding Buffer was added, and 300 mesh cell screen was passed for detection by flow cytometry.

PI staining to detect cell cycle

The tumor cell suspension was obtained using the above methods, and 50 μL PBS was retained after centrifugation. The tumor cell suspension was added with 1 mL 70% ethanol pre-cooled in an ice bath, gently beaten and mixed, fixed at 4 $^\circ\text{C}$ for 24 h, and then centrifuged at 1000 rpm for 5 min. The suspension was cleaned twice with PBS to ensure that the ethanol was completely removed. Totals of 500 μL PBS and 500 μL RNase/PI were added to resuspend the samples. The samples were incubated at 37 $^\circ\text{C}$ for 30 min in the dark,

then passed on a 300 mesh cell screen, and the samples were detected by flow cytometry.

JC-1 staining assay

The JC-1 staining working fluid was configured according to the instructions of the JC-1 mitochondrial membrane potential detection kit. A total of 500 μL JC-1 staining solution was mixed with the tumor cell suspension, and incubated in an incubator at 37 $^\circ\text{C}$ for 20 min. Then, the suspension was centrifuged at 1000 rpm for 3–4 min. The JC-1 buffer solution was added to resuspend the samples. Finally, we measured the mitochondrial membrane potential by flow cytometry.

Statistical analysis

The experimental data were showed as mean \pm standard deviation. The one-way analysis of variance (ANOVA) was performed to determine the significance of the differences between the factors via SPSS 22, and $p < 0.05$ was considered statistically significant. Origin 2018 was used to process the chart.

Results and discussion

Chemical composition analysis and molecular weight determination

We extracted the crude polysaccharide (cEFP) from *Eucommia folium* with hot water (100 $^\circ\text{C}$), alcohol precipitation and deproteinization and its yield was $4.79 \pm 0.26\%$. Then the purified polysaccharide (EFP) was separated by Sephadex G-200 gel column elution. The elute was analyzed by a UV spectrophotometer, and the sugar, protein and uronic acid contents of EFP, were $89.12 \pm 0.92\%$, $2.03 \pm 0.16\%$

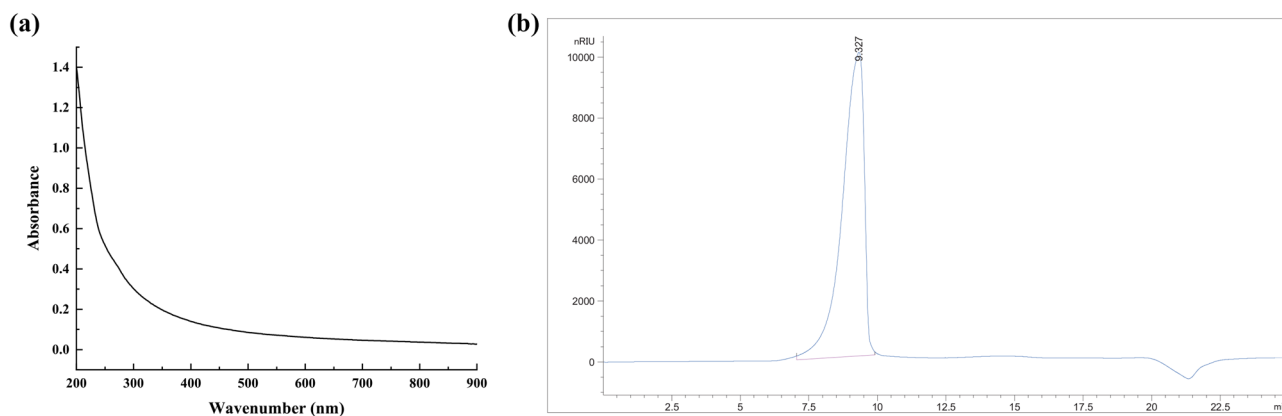


Fig. 1 (a) UV-Visible spectra of EFP. (b) HPGPC result of EFP

and $9.45 \pm 0.35\%$ respectively. EFP UV–Visible spectra (Fig. 1(a)) showed that there were no obvious absorption peaks at 260 nm and 280 nm, which proved that EFP do not contain protein and nucleic acids. A single and sharp peak was visible (Fig. 1(b)), indicating that EFP is a homogeneous polysaccharide. By establishing the standard regression equation with T-series standard dextrans ($y = -0.3173x + 8.9584$, $R^2 = 0.9923$), EFP average molecular weight was calculated as 9.98×10^5 Da ($R_t = 9.327$ min).

Monosaccharide composition analysis

The standard monosaccharides and EFP were verified by ion chromatography, and the peaks situation is shown in Fig. 2. Compared with the mixed standard curve, galactose, arabinose, glucose and galacturonic acid comprised a large part of EFP, while contents of other monosaccharides and glucuronic acid were relatively low. The molar ratios of Rha: Ara: Gal: Glc: Xyl: Man: GalA: GlcA in EFP were 0.226: 1.739: 2.183: 1: 0.155: 0.321: 0.358: 0.047, respectively, which proved that EFP is an acidic polysaccharide.

Identification of major functional groups

EFP types of functional groups and glycosidic bonds were deduced by FT-IR spectroscopy, and the result is shown in Fig. 3. EFP obvious absorption peak at 3423.67 cm^{-1} was caused by -OH tensile vibration, and the peaks at 2919.71 cm^{-1} and 1420.49 cm^{-1} correlated with the stretching vibration and the variable angle vibration of C-H, indicating that EFP has typical structural characteristics of polysaccharides [33]. The absorption peak at 1735.32 cm^{-1} showed that EFP contains ester carbonyl (-COOR) [34]. The presence of carboxylate ion (-COO⁻) in the sample can be inferred from the absorption peak at 1617.03 cm^{-1} [35], suggesting that EFP contains uronic acid, which was agreement with the result of IC analysis. The absorption peaks at 1077.24 cm^{-1} and 1023.41 cm^{-1} corresponded to C-O-H and C=O on the pyran ring [36], respectively, indicating that the pyran ring structure exists in the EFP sugar chain. The characteristic absorption peaks at 894.29 cm^{-1} and 828.19 cm^{-1} verified that EFP contains both β -type and α -type glycosidic bonds [37, 38]. These results pointed out that EFP is an acidic pyranose combining α -glycosidic and β -glycosidic bonds.

NMR derived structural characterization of EFP

To further explore EFP structural characteristics, ¹H and ¹³C were obtained for the next step of analysis. As shown in Fig. 4(a), its chemical shift was between $\delta 3.39$ – 5.42 ppm

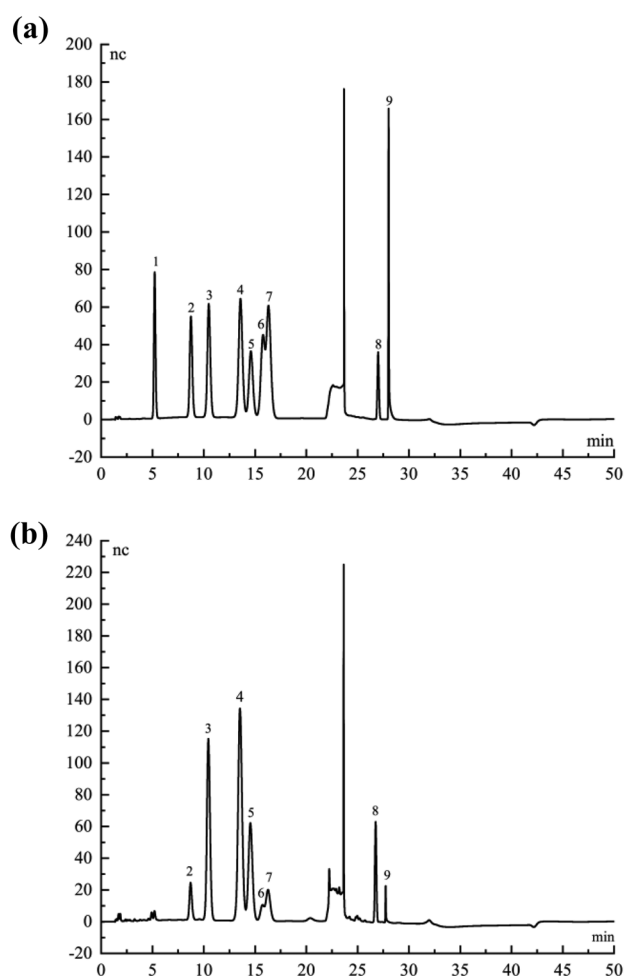


Fig. 2 Ion chromatography analysis of standard monosaccharides (a) and EFP (b). 1 fucose 2 rhamnose, 3 arabinose, 4 galactose, 5 glucose, 6 mannose, 7 xylose, 8 galacturonic acids, 9 glucuronic acids

in ¹H NMR, which was a typical signal for polysaccharides [39]. The results also showed that EFP had α -type and β -type glycosidic bonds. The chemical shift of 4.79 ppm was attributed to the characteristic peak of the solvent D₂O, and 3.39–4.39 ppm was attributed to the proton signal of H2-H6 [40]. The signals at 1.26 and 1.30 ppm were sourced from the H-6 of rhamnose, and the methyl group was attributed to rhamnose C-6, which can be confirmed by the cross peak 1.23/17.42 ppm in the HSQC spectrum (Fig. 4(d)). The chemical shift information of H-5 in rhamnose can be obtained from the cross peak of H-5/H-6 in the COSY spectrum (Fig. 4(c)). Due to rhamnose low content, the chemical shifts of other protons needed further analysis and research, which could not be completely obtained from the COSY spectrum. The signal at 2.10–2.20 ppm was assigned to the proton on the O-acetyl group, the 20.49 ppm on the ¹³C signal assigned to the methyl carbon signal on the O-acetyl group, and the downfield signal at 173.30 ppm was labeled

as the signal on the O-acetyl group, which is the C-6 of the uronic acid, indicating the presence of uronic acid in EFP [41]. The signal peak at 69.39 ppm was caused by the presence of the methoxy group, which was also confirmed by the absorption peak at 3.39–3.57 ppm observed in the ^1H spectrum [34]. Based on relevant studies, the signal at 5.17/109.94 ppm was assigned to $\alpha\text{-L-Ara}$ [42], the signal at 4.55/105.65 ppm to $\beta\text{-D-Gal}$ [28], and the signal at 4.39/102.91 ppm indicated the presence of $\beta\text{-D-Glc}$ [30]. Other proton and carbon signals needed to be assigned by COSY and HSQC.

In the ^{13}C NMR spectrum (Fig. 4(b)), two higher signals were found in the region around 109 ppm. Because arabinose usually exists as furanose in natural plant polysaccharides [43], these two signals were assigned to $\alpha\text{-L-Ara}$. The two main peaks at 109.94 ppm and 110.03 ppm corresponded to $\alpha\text{-L-Araf-(1}\rightarrow\text{)}$ (residue A) and $\rightarrow\text{3,5)-}\alpha\text{-L-Araf-(1}\rightarrow\text{)}$ (residue B) linked C-1, respectively. A 5.17 ppm signal corresponded to H-1 of residue A, 4.18 ppm, 3.91 ppm, 4.08 ppm corresponded to H-2, H-3 and H-4 of residue A, and signal 3.87 ppm corresponded to H-5 of residue A. The carbon signal of residue A in the HSQC spectrum was easily assigned based on the ^1H NMR assignment from the COSY spectrum. Cross peaks 4.18/81.40 ppm, 3.91/76.53 ppm, 4.08/84.05 ppm and 3.87/61.17 ppm corresponded to residues A's H-2/C-2, H-3/C-3, H-4/C-4 and H-5/C-5. Residue B was identified in the same way, and the specific results are shown in Table 1.

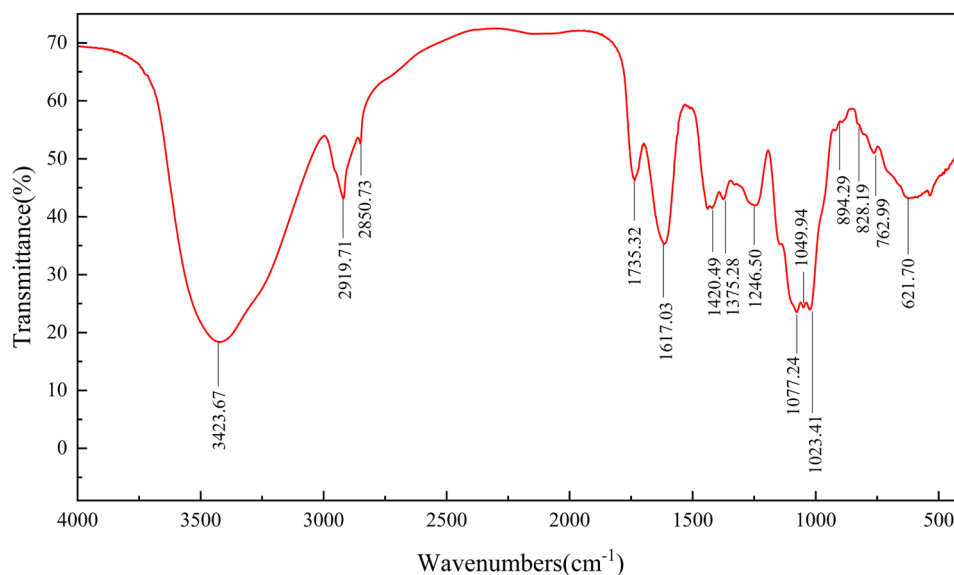
Residue C appeared to be galactose in the β -anomeric configuration for a low-field anomeric proton of 4.55 ppm and a relatively high-field anomeric carbon signal of 105.65 ppm. A partial proton signal for residue C was obtained from the COSY spectrum, and the corresponding ^{13}C signal was identified by the HSQC spectrum. The

partial proton signals of residue C were obtained from the COSY spectrum, while the corresponding ^{13}C signals were identified by the HSQC spectrum, indicating that residue C is $\rightarrow\text{3)-}\beta\text{-Galp-(1}\rightarrow\text{.}\rightarrow\text{3,6)-}\beta\text{-GlcP-(1}\rightarrow\text{)}$ (residue D) and has a signal of 4.39 ppm in the anomeric region in the ^1H spectrum. Based on the cross peaks of adjacent protons, the chemical shift of H-2 in residue D was obtained from the signal at 4.39/3.39 ppm in the COSY spectrum. Additionally, a series of cross peaks were obtained as 3.39/3.52 ppm, 3.52/3.60 ppm, and 3.60/3.82 ppm, respectively. According to the cross peaks in the HSQC spectrum, the chemical shifts of C-1 and C-5 were δ 103.33, δ 73.55, δ 80.01, δ 73.21, and δ 74.42. In the ^1H NMR spectrum, 5.27 ppm was assigned to $\alpha\text{-D-Man}$. Based on the proton signal, the chemical shift from the C-1 carbon was identified as 100.95 ppm from the HSQC spectrum. The H-2 to H-6 and C-2 to C-6 signals were further identified in combination with COSY. Analysis of the C-1 downfield relative to standard values and analogy with the literature data showed that residue E is $\rightarrow\text{2)-}\alpha\text{-D-Manp-(1}\rightarrow\text{)}$. In conclusion, the NMR results were consistent with the results of the monosaccharide composition analysis and FT-IR spectroscopy.

Microscopic surface structure analysis

EFP apparent morphology at different magnifications can be observed by scanning electron microscopy. The structure of polysaccharides under the SEM was 1000 \times , 2000 \times and 3500 \times , respectively (Fig. 5). It can be observed that EFP presents a dense, smooth and curled reticular structure with different mesh sizes at the micron level. This structure may be formed by the cross-linking and aggregation between the molecular chains of polysaccharides.

Fig. 3 FT-IR spectrum of EFP



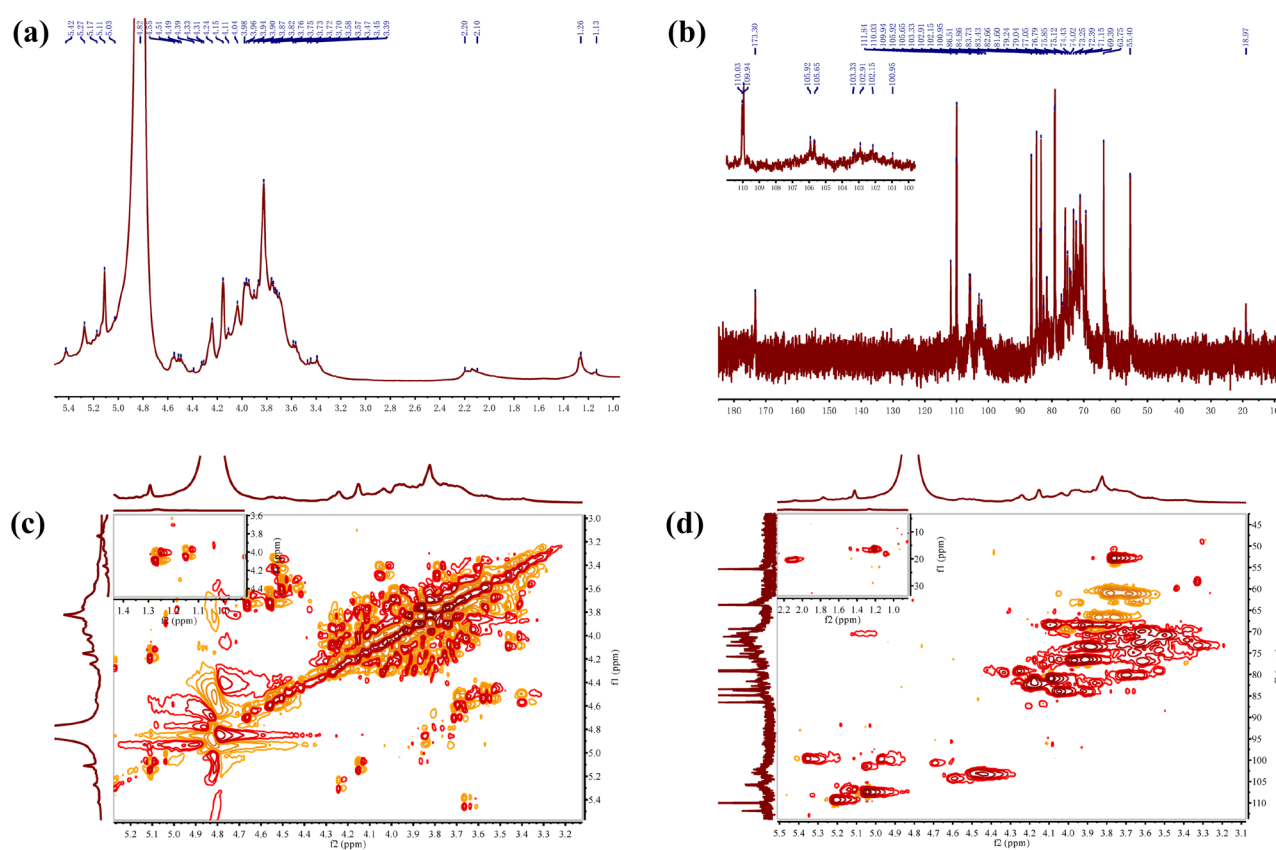


Fig. 4 (a) ^1H NMR spectrum of EFP. (b) ^{13}C NMR spectrum. (c) COSY spectrum. (d) HSQC spectrum. of EFP

Triple helix identification

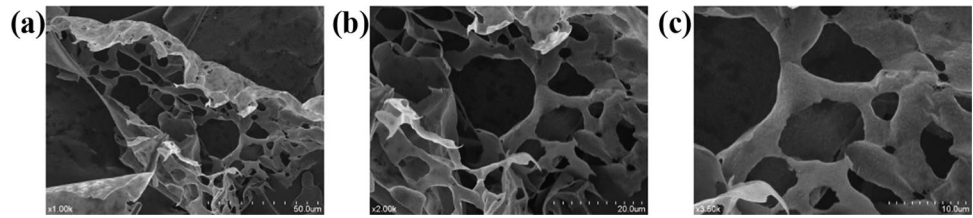
The polysaccharides' molecular conformation affects their three-dimensional shape in solution. If there is a triple helix structure in EFP, its λ_{max} will be red-shifted in the Congo red

alkaline solution [44]. After mixing EFP with the Congo red alkaline solution, the absorption wavelength decreased with the increase of NaOH concentration, and there was no obvious red shift of λ_{max} (Fig. 6). Therefore, EFP do not have a three-helix conformation.

Table 1 NMR assignments of sugar residues from EFP

Residue	Chemical shift(ppm)					
	C1/H1	C2/H2	C3/H3	C4/H4	C5/H5	C6/H6
A: $\alpha\text{-L-Araf-}(1 \rightarrow$	109.94	81.40	76.53	84.05	61.17	
	5.17	4.18	3.91	4.08	3.87	
B: $\rightarrow 3,5\text{-}\alpha\text{-Araf-}(1 \rightarrow$	110.03	82.27	84.20	81.06	67.44	
	5.11	4.14	4.01	4.23	3.74/3.82	
C: $\rightarrow 3\text{-}\beta\text{-Galp-}(1 \rightarrow$	105.65	72.35	84.39	69.20	69.02	61.17
	4.55	3.57	3.78	4.10	3.93	3.63/3.77
D: $\rightarrow 3,6\text{-}\beta\text{-GlcP-}(1 \rightarrow$	103.33	73.55	80.01	73.21	74.42	
	4.39	3.39	3.52	3.60	3.82	
E: $\rightarrow 2\text{-}\alpha\text{-D-Manp-}(1 \rightarrow$	100.95	78.99	70.08	66.76	74.42	61.17
	5.27	4.21	3.97	3.65	3.56	3.51/3.46
F: $\rightarrow 4\text{-}\alpha\text{-GalpA-}(1 \rightarrow$	102.15	-	69.02	78.80	-	173.30
	5.03	3.89	4.11	4.32	4.20	-
G: $\rightarrow 2,4\text{-}\alpha\text{-Rhap-}(1 \rightarrow$	-	-	83.36	-	68.78	17.42
	-	-	3.94	3.71	4.01	1.13/1.23

Fig. 5 SEM images of EFP (1000 \times , 2000 \times , 3500 \times)



Anti-tumor activity in H22 tumor-bearing mice

Effects on mice body weight and solid tumors

Mice body weight is an important indicator in measuring the toxicity and side effects of a drug therapy. As illustrated in Table 2, the weight of mice in each group was about 20 g at the beginning. In the last week of the experiment, the weight gain of the model group was less than that of the blank group ($p < 0.05$). During this experiment, the mice in the model group showed an obvious slowdown in activity and a loss of appetite, indicating that the solid tumors had a great impact on the physical and mental states of mice. In the later stage of the experiment, the mice were lethargic and listless, and some even died. Meanwhile, the mice treated with EFP were in good living conditions with the obvious weight gain ($p < 0.05$), especially in the 300 mg/kg dose group.

EFP anti-tumor effect was further evaluated by measuring tumors' weight and volume. The experimental results of the different groups are shown in the Fig. 7(a). It can be observed that the tumors' weight and volume in the model group were much higher than those in the treatment groups ($p < 0.05$). Compared to the model group, the tumors' weight and volume in the EFP treatment groups significantly decreased obviously ($p < 0.05$). The tumor inhibition rates in the 100 mg/kg EFP and 300 mg/kg EFP groups reached 21.43% and 46.54%, respectively. Above all, EFP inhibited the proliferation of H22 tumors in a dose-dependent manner. Although the 5-Fu group had a higher tumor inhibition rate (64.25%), it also had more serious side effects when in considering the mice body weight. In contrast, EFP not only inhibited the growth of tumors but also had almost no negative effects on the body.

Effects on immune indexes

The spleen and thymus are the largest immune organs and central lymphatic organs of the body. They are also the sites of T cell maturation and differentiation, and therefore, are of great significance for various lymphocytes in the immune system [45]. In this study, the thymus and spleen indexes were measured to further determine whether EFP was cytotoxic. As shown in Fig. 7(b), although 5-Fu significantly inhibited tumor growth, both thymus and spleen

indexes were at low levels ($p < 0.05$), which may be due to its greater toxicity and its immunosuppressive effect [46]. However, after EFP gavage treatment, the mice immune organ index improved, particularly, the thymus index of the high-dose group, which was markedly better than that of the model group ($p < 0.05$). Moreover, the spleen index was also significantly declined ($p < 0.05$), suggesting that EFP can achieve a better tumor suppression effect without affecting the immune system of H22 tumor-bearing mice.

Effects of EFP on tumor and liver tissues

Hematoxylin and Eosin staining (H&E staining) is the most basic and widely used technique in histological and pathological studies. Hematoxylin staining solution can make the nucleus purple blue; while Eosin gives the cytoplasm and extracellular matrix a red color [47]. Therefore, we analyzed morphological changes in tumor tissues and liver sections from different treatment groups. We observed that the tumor tissue cells in the model group are closely arranged and have a complete cell morphology (Fig. 8(a)). After EFP treatment, the tumor cells were damaged at different degrees in a dose-dependent manner. After high-dose EFP gavage treatment, the tumor tissues were sparsely arranged, and the nuclear morphology was irregular, with karyopyknosis, nuclear fragmentation and other phenomena, which might have been

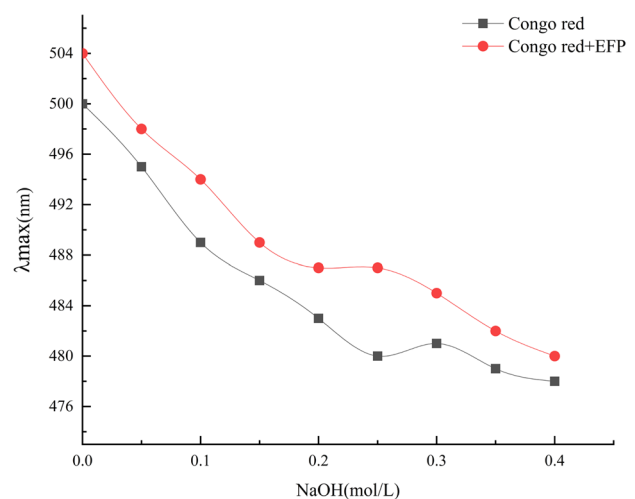


Fig. 6 The maximum absorption wavelength of Congo red and EFP at various concentrations of sodium hydroxide solution

Table 2 Effect of EFP on the body weight of H22 tumor-bearing mice

	Dosage(mg/kg/D)	Body weight(g)		Average weight increment(g)	Number of mice(start/end)
		Initial weight	Final weight		
Blank	-	21.13 ± 0.90	33.75 ± 0.85	12.62 ± 0.98	10/10
Model	-	20.91 ± 1.08	31.86 ± 0.87*	10.95 ± 1.26*	10/9
5-Fu	20	20.75 ± 1.29	26.01 ± 0.77#	5.26 ± 1.43#	10/7
EFP	100	21.35 ± 0.96	32.57 ± 0.91	11.22 ± 0.60	10/10
	300	22.09 ± 0.52	34.34 ± 1.08#	12.25 ± 1.12#	10/10

* $p < 0.05$ compared to blank group

$p < 0.05$ compared to model group

caused by inflammatory cell infiltration. These phenomena were similar to the results of the 5-Fu group.

As shown in Fig. 8(b), the liver cells of normal mice were closely arranged, with a normal cell morphology and a clear nuclear structure. However, in the model group, the morphology of the cells was damaged, the nucleus shifted, and the cytoplasmic space expanded. In the liver tissue, inflammatory cell infiltration, hepatocyte edema, and necrosis were observed. Compared with the model group, the population of necrotic cells in the EFP treatment group was reduced in a dose-dependent manner. The liver cells of the high-dose group were densely arranged with regular cell shape,

indicating that there was no obvious toxicity associated with the high-dose EFP treatment. The sparsely arranged liver tissues, incomplete cell membranes, karyopyknosis, fragmentation, and other hepatic necrosis phenomena in the 5-fu treated group of mice, indicated that 5-Fu damaged the mice liver, leading to a local necrosis of the liver tissue.

Detection of EFP-induced tumor cell apoptosis by Annexin V-FITC/PI double staining

In normal cells, phosphatidylserine (PS) is located on the inner side of the cells' membrane. When cells are in the early

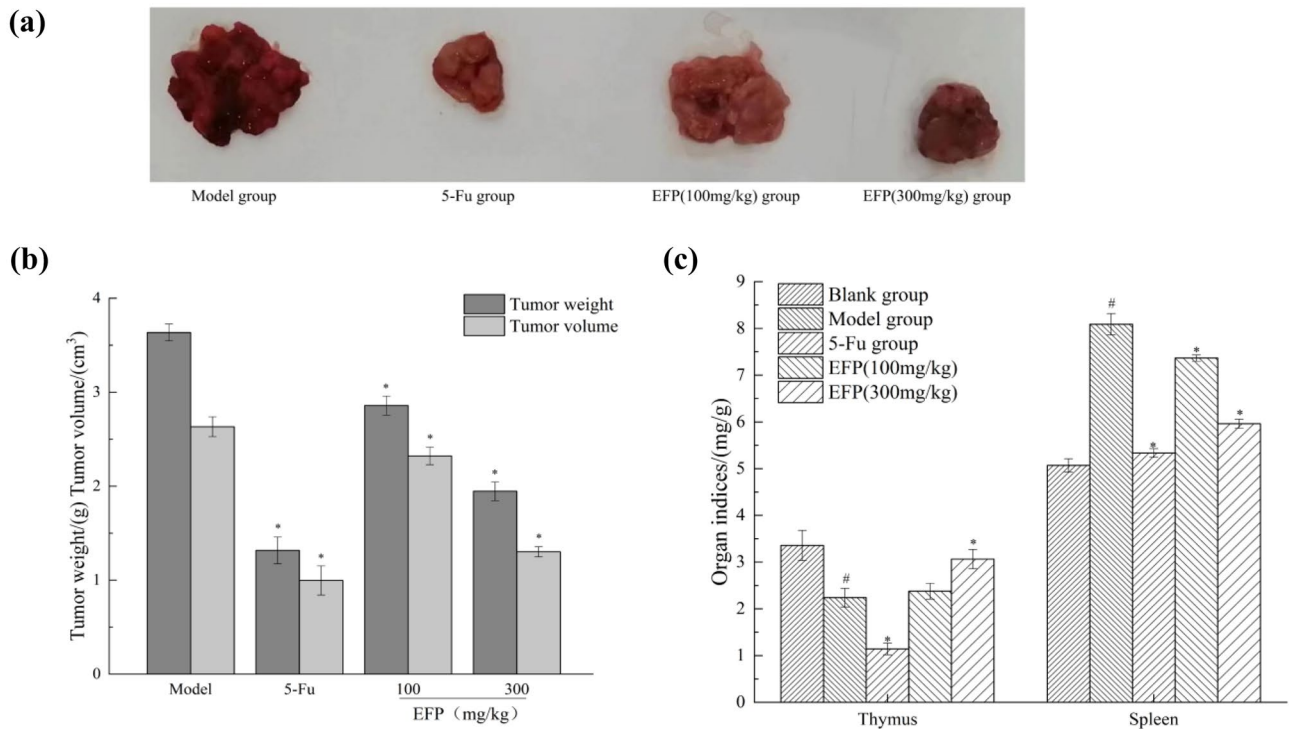


Fig. 7 (a) Anatomical diagram of the tumors in each group. (b) Tumor weight and volume. (c) Immune organ indices. # $p < 0.05$ compared to the blank group, * $p < 0.05$ compared to model group

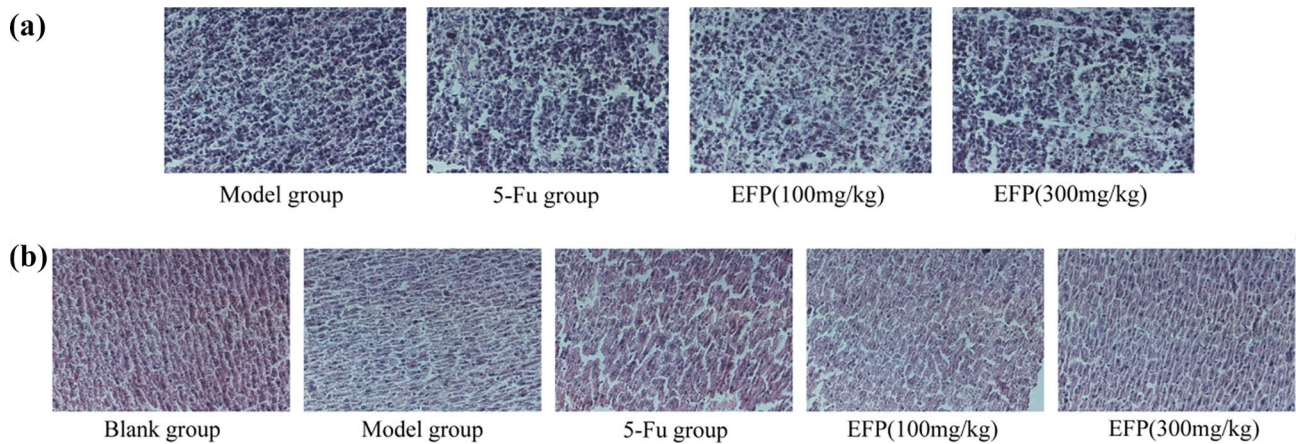


Fig. 8 H&E staining results of solid tumors and liver paraffin sections of tumor-bearing mice ($\times 20$): (a: H&E staining of mice solid tumors sections, b: H&E staining of mice liver sections)

stage of apoptosis, PS can transfer from inside the cell membrane to surface. As a Ca^{2+} -dependent phospholipid binding protein, Annexin V can combine with PS and has a better affinity. Propidium iodide (PI) is a nucleic acid dye, that can penetrate the membranes of cells at apoptotic metaphase, later phase and necrotic cells, resulting in a red staining of the nucleus [48]. Therefore, Annexin V-FITC/PI apoptosis detection kit is capable to distinguish cells in the early and late stages of apoptosis. As shown in the Fig. 9, 84% of normal cells in the model group demonstrated that the tumor tissue was in good condition. After 100 mg/kg EFP treatment, the apoptosis rate increased from 12.37% to 30.3%. With 300 mg/kg EFP treatment, the apoptotic rate increased to 42%, and

the degree of tumor cell necrosis after EFP treatment also showed a dose-dependent increase. Meanwhile, significant apoptosis and necrosis were observed in the 5-Fu group.

Cell cycle analysis

Double-stranded DNA can combine with pyridine iodide (PI) and produce fluorescence. Moreover, the fluorescence intensity and the content of double-stranded DNA are directly proportional [49]. After PI staining, the cell cycle can be tested by flow cytometry based on the distribution of DNA content. As shown in Fig. 10, after EFP treatment, the percentage of cells in the S phase increased from 16% to 29.67% (100 mg/

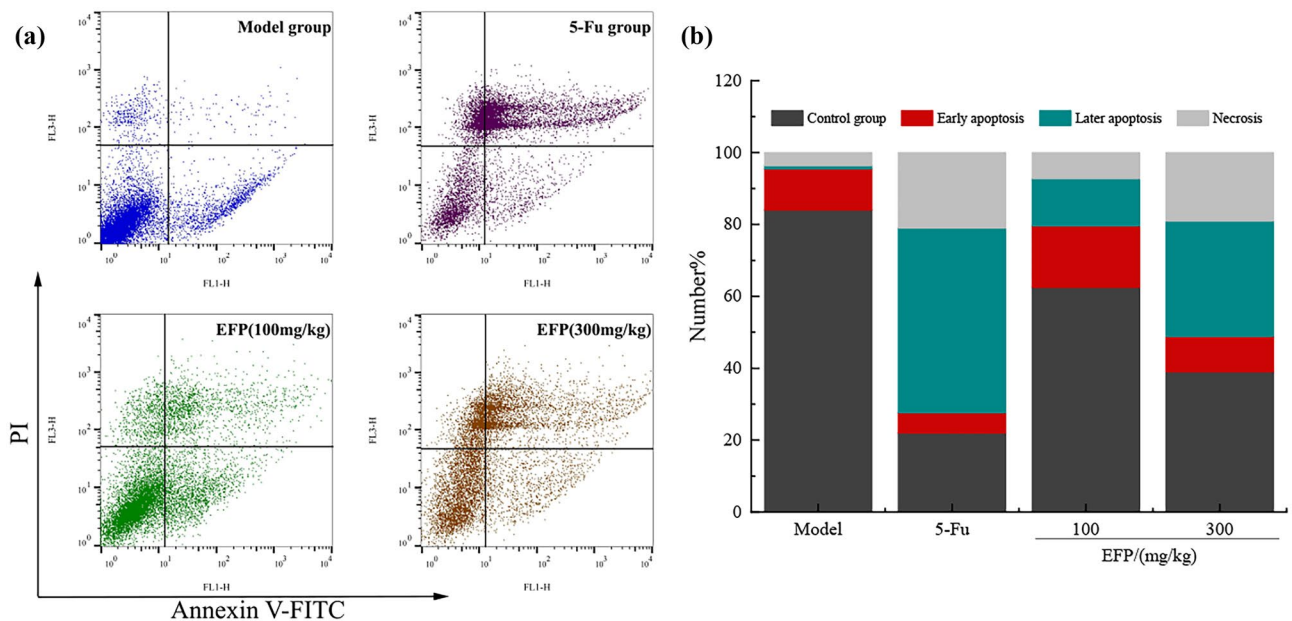


Fig. 9 (a) Cell apoptosis results of solid tumor detected by the flow cytometer. (b) The proportion of apoptotic and necrotic cells in different treatment groups

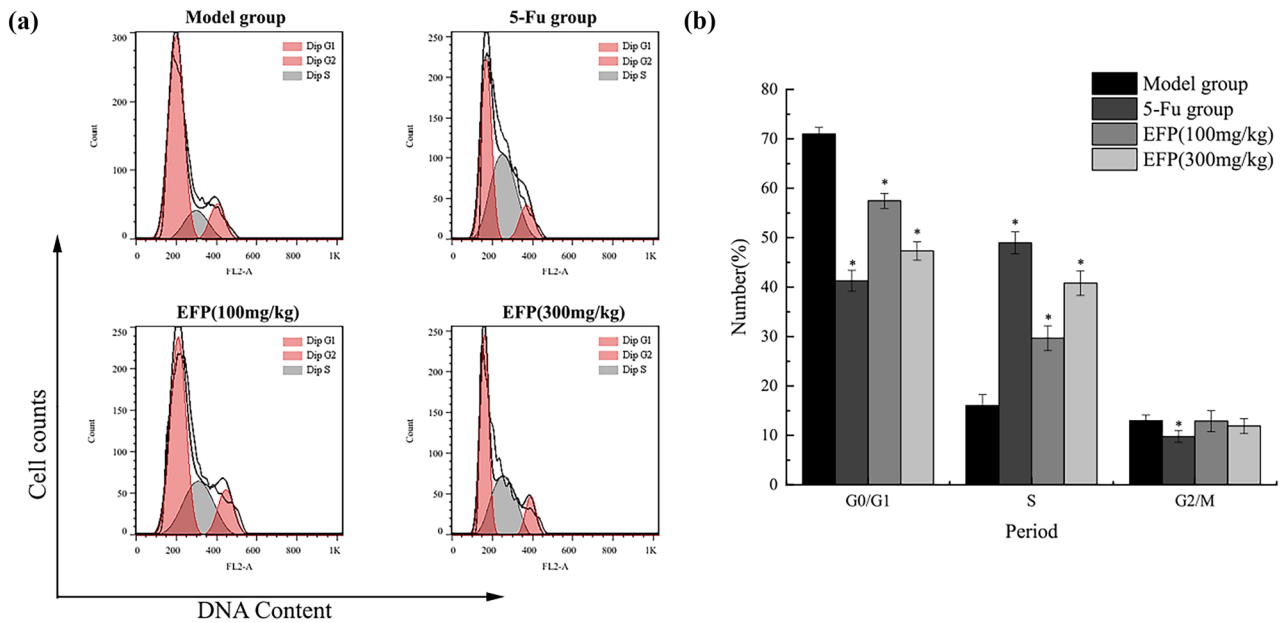


Fig. 10 (a) Flow cytometry detection of the cell cycle of solid tumor cells. (b) Histogram of cell proportions in different periods. * $p < 0.05$ compared to the model group

kg) and 40.8% (300 mg/kg) compared with that of the model group. Meanwhile, the ratio of G0/G1 cells was also significantly decreased. This indicated that EFP can delay the cell cycle in the S phase following treatment through affecting DNA replication and proliferation of tumor cells.

Effects of EFP on tumor cells’ mitochondrial membrane potential

A decrease in mitochondrial membrane potential can be determined by detecting the conversion of JC-1 from red

fluorescence to green fluorescence [30]. This is an indicative event in early stages of apoptosis. As shown in Fig. 11, after EFP treatment, the signal peak shifted to the left. The low-dose group (EFP, 100 mg/kg) was contrasted with the model group, and the proportion of strong fluorescent cells decreased from 87.3% to 73.9%, while the proportion of strong fluorescent cells in the high-dose group (EFP, 300 mg/kg) decreased to 59.2%, indicating that EFP causes a decrease in mitochondrial membrane potential in a dose-dependent manner. The decrease indicated mitochondrial damage, which is an irreversible step of cell apoptosis, and

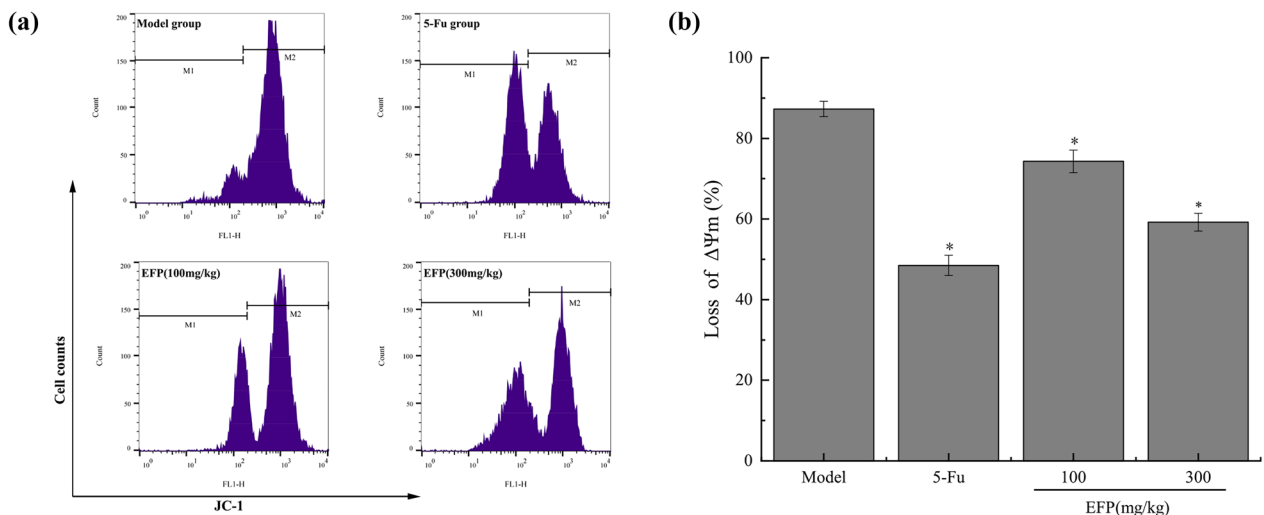


Fig. 11 (a) JC-1 staining results were detected by flow cytometry. (b) Histogram of changes in mitochondrial membrane potential in different groups. * $p < 0.05$ compared to the model group

thus provides evidence that EFP can induce apoptosis of tumor cells.

Conclusion

To date, there are few studies on *Eucommia folium* polysaccharides. Xu et al. [19] analyzed the molecular weight (Mw) of polysaccharides from *Eucommia ulmoides* Oliver leaf (EULP) and found that it is 38830 g/mol. This may be due to different methods of extraction and purification. Glucose was the dominant sugar component (38.2–39.1%) of EULP that belongs to a structure of β -type acidic heteropolysaccharides. In this study, a water-soluble acidic polysaccharide (EFP) was extracted and purified. HPGPC verified that the average molecular weight of EFP is 9.98×10^5 Da. It has been shown that high molecular weight polysaccharides may be related to their anti-tumor activity [50, 51]. We also found that arabinose, galactose, and glucose were the main EFP monosaccharides. The results of infrared spectrum analysis confirmed that EFP is a heteropolysaccharide, containing pyranose with both α -glycosidic and β -glycosidic bonds. When combining these results with NMR spectroscopy, EFP was mainly composed of α -L-Araf-(1 \rightarrow , \rightarrow 3,5)- α -Araf-(1 \rightarrow , \rightarrow 3)- β -Galp-(1 \rightarrow , \rightarrow 3,6)- β -GlcP-(1 \rightarrow , \rightarrow 2)- α -D-Manp-(1 \rightarrow , \rightarrow 4)- α -GalpA-(1 \rightarrow and \rightarrow 2,4)- α -Rhap-(1 \rightarrow .

In addition, through the analysis of EFP antitumoral activity in mice, we showed that EFP can effectively inhibit the growth of tumors, block the proliferation of tumor cells at the S phase, destroy cell mitochondria and induce the apoptosis of H22 carcinoma cells. Although few, the studies on the biological activity of *Eucommia folium* polysaccharides were more focused on its antioxidant and immune activities. According to the relevant information, this is the first study that analyzed the anti-hepatoma activity of *Eucommia folium* polysaccharide. Previous studies [18] confirmed that *Eucommia ulmoides* polysaccharide (EUPS) can significantly enhance lymphocyte proliferation and cytokine production *in vitro*. *In vivo* experiments, EUPS can significantly improve specific antibody titers and T cell proliferation. These results suggest that EUPS is a potent immune stimulator. In conclusion, EFP can be regarded as a potential medicine for the prevention and primary treatment of liver cancer, which provides a new possibility for the development of anticancer drugs based on the above research. Furthermore, EFP higher structure characterization and *in vivo* antitumoral mechanism are worthy of further studies.

Authors contribution Zhi-Qian Yan: Conceptualization, Investigation, Data curation, Writing-Original draft preparation, Writing-Reviewing and Editing. Su-Yun Ding: Methodology. Pei Chen: Software, Formal analysis. Hui-Ping Liu: Resources, Project administration, Funding acquisition. Meng-Li Chang: Software, Validation. Shu-Yuan Shi: supervised.

Funding This research was supported by National Natural Science Foundation of China (No.31801568).

Data availability statement The datasets generated during and/or analysed during the current study are available from the corresponding author on reasonable request.

Compliance with ethical standards

Conflicts of interest/Competing interests We declare that we have no financial and personal relationships with other people or organizations that can inappropriately influence our work, there is no professional or other personal interest of any nature or kind in any products, service and/or company that could be construed as influencing the position presented in, or the review of, the manuscript entitled

Ethical approval The animal experiments were conducted in accordance with the Regulations on the Administration of Laboratory Animals

References

1. Wang, C.J., Guo, X., Zhai, R.Q., Sun, C., Xiao, G., Chen, J., Wei, M.Y., Shao, C.L., Gu, Y.: Discovery of penipanoid C-inspired 2-(3,4,5-trimethoxybenzoyl)quinazolin-4(3H)-one derivatives as potential anticancer agents by inhibiting cell proliferation and inducing apoptosis in hepatocellular carcinoma cells. *Eur J Med Chem* **224**, 113671 (2021). <https://doi.org/10.1016/j.ejmech.2021.113671>
2. Zhang, C., Li, L.L., Hou, S., Shi, Z.H., Xu, W.J., Wang, Q., He, Y.H., Gong, Y.F., Fang, Z.R., Yang, Y.: Astragaloside IV inhibits hepatocellular carcinoma by continually suppressing the development of fibrosis and regulating pSmad3C/3L and Nrf2/HO-1 pathways. *J Ethnopharmacol* **279**, 114350 (2021). <https://doi.org/10.1016/j.jep.2021.114350>
3. Zhu, Q.W., Chen, J.H., Li, Q., Wang, T., Li, H.B.: Antitumor activity of polysaccharide from *Laminaria japonica* on mice bearing H22 liver cancer. *Int J Biol Macromol* **92**, 156–158 (2016). <https://doi.org/10.1016/j.ijbiomac.2016.06.090>
4. Li, W.Z., Wang, Y.F., Zhou, X.B., Pan, X.H., Lü, J.H., Sun, H.L., Xie, Z.P., Chen, S.Y., Gao, X.: The anti-tumor efficacy of 20(S)-protopanaxadiol, an active metabolite of ginseng, according to fasting on hepatocellular carcinoma. *J Ginseng Res.* **46**(1), 167–174 (2021). <https://doi.org/10.1016/j.jgr.2021.06.002>
5. Trojan, J., Zangos, S., Schnitzbauer, A.A.: Diagnostics and Treatment of Hepatocellular Carcinoma in 2016: Standards and Developments. *Visc Med* **32**(2), 116–120 (2016). <https://doi.org/10.1159/000445730>
6. Chen, P., Liu, H.P., Ji, H.H., Sun, N.X., Feng, Y.Y.: A cold-water soluble polysaccharide isolated from *Grifola frondosa* induces the apoptosis of HepG2 cells through mitochondrial passway. *Int J Biol Macromol* **125**, 1232–1241 (2019). <https://doi.org/10.1016/j.ijbiomac.2018.09.098>
7. Mao, G.H., Zhang, Z.H., Fei, F., Ding, Y.Y., Zhang, W.J., Chen, H., Ali, S.S., Zhao, T., Feng, W.W., Wu, X.Y., Yang, L.Q.: Effect of *Grifola frondosa* polysaccharide on anti-tumor activity in combination with 5-Fu in Heps-bearing mice. *Int J Biol Macromol* **121**, 930–935 (2019). <https://doi.org/10.1016/j.ijbiomac.2018.10.073>
8. Zhao, T., Mao, G.H., Zhang, M., Zou, Y., Feng, W.W., Gu, X.Y., Zhu, Y., Mao, R.W., Yang, L.Q., Wu, X.Y.: Enhanced antitumor and reduced toxicity effect of *Schisanreia* polysaccharide in 5-Fu

- treated Heps-bearing mice. *Int J Biol Macromol* **63**, 114–118 (2014). <https://doi.org/10.1016/j.ijbiomac.2013.10.037>
9. Torbenson, M.S.: Hepatocellular carcinoma: making sense of morphological heterogeneity, growth patterns, and subtypes. *Hum Pathol* **112**, 86–101 (2021). <https://doi.org/10.1016/j.humpath.2020.12.009>
 10. Zhao, Y.N., Sun, H.Y., Ma, L., Liu, A.J.: Polysaccharides from the peels of *Citrus aurantifolia* induce apoptosis in transplanted H22 cells in mice. *Int J Biol Macromol* **101**, 680–689 (2017). <https://doi.org/10.1016/j.ijbiomac.2017.03.149>
 11. Khan, T., Date, A., Chawda, H., Patel, K.: Polysaccharides as potential anticancer agents-A review of their progress. *Carbohydr Polym* **210**, 412–428 (2019). <https://doi.org/10.1016/j.carbpol.2019.01.064>
 12. Wang, N.F., Wu, Y., Jia, G.G., Wang, C.L., Xiao, D.G., Goff, H.D., Guo, Q.B.: Structural characterization and immunomodulatory activity of mycelium polysaccharide from liquid fermentation of *Monascus purpureus* (Hong Qu). *Carbohydr Polym* **262**, 117945 (2021). <https://doi.org/10.1016/j.carbpol.2021.117945>
 13. Liu, Y., Zhang, J.J., Meng, Z.L.: Purification, characterization and anti-tumor activities of polysaccharides extracted from wild *Russula griseocarnosa*. *Int J Biol Macromol* **109**, 1054–1060 (2018). <https://doi.org/10.1016/j.ijbiomac.2017.11.093>
 14. Niu, J.F., Wang, S.P., Wang, B.L., Chen, L.J., Zhao, G.M., Liu, S., Wang, S.Q., Wang, Z.Z.: Structure and anti-tumor activity of a polysaccharide from *Bletilla ochracea* Schltr. *Int J Biol Macromol* **154**, 1548–1555 (2020). <https://doi.org/10.1016/j.ijbiomac.2019.11.039>
 15. Li, H.H., Mi, Y., Duan, Z.G., Ma, P., Fan, D.D.: Structural characterization and immunomodulatory activity of a polysaccharide from *Eurotium cristatum*. *Int J Biol Macromol* **162**, 609–617 (2020). <https://doi.org/10.1016/j.ijbiomac.2020.06.099>
 16. Li, W.F., Hu, X.Y., Wang, S.P., Jiao, Z.R., Sun, T.Y., Liu, T.Q., Song, K.D.: Characterization and anti-tumor bioactivity of astragalus polysaccharides by immunomodulation. *Int J Biol Macromol* **145**, 985–997 (2020). <https://doi.org/10.1016/j.ijbiomac.2019.09.189>
 17. Xie, J.H., Tang, W., Jin, M.L., Li, J.E., Xie, M.Y.: Recent advances in bioactive polysaccharides from *Lycium barbarum* L., *Zizyphus jujuba* Mill., *Plantago* spp., and *Morus* spp.: Structures and functionalities. *Food Hydrocolloids* **60**, 148–160 (2016). <https://doi.org/10.1016/j.foodhyd.2016.03.030>
 18. Feng, H.B., Fan, J., Song, Z.H., Du, X.G., Chen, Y., Wang, J.S., Song, G.D.: Characterization and immunoenhancement activities of *Eucommia ulmoides* polysaccharides. *Carbohydr Polym* **136**, 803–811 (2016). <https://doi.org/10.1016/j.carbpol.2015.09.079>
 19. Xu, J.K., Hou, H.J., Hu, J.P., Liu, B.C.: Optimized microwave extraction, characterization and antioxidant capacity of biological polysaccharides from *Eucommia ulmoides* Oliver leaf. *Sci Rep* **8**(1), 6561 (2018). <https://doi.org/10.1038/s41598-018-24957-0>
 20. Huang, W., Xue, A., Niu, H., Jia, Z., Wang, J.W.: Optimised ultrasonic-assisted extraction of flavonoids from *Folium eucommiae* and evaluation of antioxidant activity in multi-test systems in vitro. *Food Chem.* **114**(3), 1147–1154 (2009). <https://doi.org/10.1016/j.foodchem.2008.10.079>
 21. Ren, X.M., Han, Z.Z., Song, L.X., Lv, Z.Y., Yang, Y.B., Xiao, Y., Zhang, Z.-J.: Four new phenolic compounds from the tender leaves of *Eucommia ulmoides* Oliv. and their anti-inflammatory activities. *Phytochem Lett* **44**, 173–177 (2021). <https://doi.org/10.1016/j.phytol.2021.06.020>
 22. Xing, Y.F., He, D., Wang, Y., Zeng, W., Zhang, C., Lu, Y., Su, N., Kong, Y.H., Xing, X.H.: Chemical constituents, biological functions and pharmacological effects for comprehensive utilization of *Eucommia ulmoides* Oliver. *Food Sci. Human Wellness* **8**(2), 177–188 (2019). <https://doi.org/10.1016/j.fshw.2019.03.013>
 23. Deng, Y.Q., Ma, F.B., Ruiz-Ortega, L.I., Peng, Y., Tian, Y., He, W.Q., Tang, B.: Fabrication of strontium *Eucommia ulmoides* polysaccharides and in vitro evaluation of their osteoimmunomodulatory property. *Int J Biol Macromol* **140**, 727–735 (2019). <https://doi.org/10.1016/j.ijbiomac.2019.08.145>
 24. Tian, W.T., Zhang, X.W., Liu, H.P., Wen, Y.H., Li, H.R., Gao, J.: Structural characterization of an acid polysaccharide from *Pinellia ternata* and its induction effect on apoptosis of Hep G2 cells. *Int J Biol Macromol* **153**, 451–460 (2020). <https://doi.org/10.1016/j.ijbiomac.2020.02.219>
 25. Dubois, M., Gilles, K.A., Hamilton, J.K., Rebers, P.A.: Colorimetric Method for Determination of Sugars and Related Substances. *Anal. Chem.* **28**(3), 350–356 (1956). <https://doi.org/10.1021/ac60111a017>
 26. Bradford, M.M.: A rapid and sensitive method for the quantification of microgram quantities of protein utilizing the principle of protein dye-binding. *Anal. Biochem.* **72**(1–2), 248–254 (1976). [https://doi.org/10.1016/0003-2697\(76\)90527-3](https://doi.org/10.1016/0003-2697(76)90527-3)
 27. Bitter, T., Muir, H.M.: A modified uronic acid carbazole reaction. *Anal. Biochem.* **4**(4), 330–334 (1962). [https://doi.org/10.1016/0003-2697\(62\)90095-7](https://doi.org/10.1016/0003-2697(62)90095-7)
 28. Gu, S.S., Sun, H.Q., Zhang, X.L., Huang, F.N., Pan, L.C., Zhu, Z.Y.: Structural characterization and inhibitions on α -glucosidase and α -amylase of alkali-extracted water-soluble polysaccharide from *Annona squamosa* residue. *Int J Biol Macromol* **166**, 730–740 (2021). <https://doi.org/10.1016/j.ijbiomac.2020.10.230>
 29. Zhang, S., Song, Z., Shi, L., Zhou, L., Zhang, J., Cui, J., Li, Y., Jin, D.Q., Ohizumi, Y., Xu, J., Guo, Y.: A dandelion polysaccharide and its selenium nanoparticles: Structure features and evaluation of anti-tumor activity in zebrafish models. *Carbohydr Polym* **270**, 118365 (2021). <https://doi.org/10.1016/j.carbpol.2021.118365>
 30. Wang, Q., Niu, L.L., Liu, H.P., Wu, Y.R., Li, M.Y., Jia, Q.: Structural characterization of a novel polysaccharide from *Pleurotus citrinopileatus* and its antitumor activity on H22 tumor-bearing mice. *Int J Biol Macromol* **168**, 251–260 (2021). <https://doi.org/10.1016/j.ijbiomac.2020.12.053>
 31. Guo, X.Y., Kang, J., Xu, Z.Y., Guo, Q.B., Zhang, L.F., Ning, H.F., Cui, S.W.: Triple-helix polysaccharides: Formation mechanisms and analytical methods. *Carbohydr Polym* **262**, 117962 (2021). <https://doi.org/10.1016/j.carbpol.2021.117962>
 32. Feng, Y.Y., Ji, H.Y., Dong, X.D., Yu, J., Liu, A.J.: Polysaccharide extracted from *Atractylodes macrocephala* Koidz (PAMK) induce apoptosis in transplanted H22 cells in mice. *Int J Biol Macromol* **137**, 604–611 (2019). <https://doi.org/10.1016/j.ijbiomac.2019.06.059>
 33. Wang, X.T., Zhu, Z.Y., Zhao, L., Sun, H.Q., Meng, M., Zhang, J.Y., Zhang, Y.M.: Structural characterization and inhibition on α -d-glucosidase activity of non-starch polysaccharides from *Fagopyrum tartaricum*. *Carbohydr Polym* **153**, 679–685 (2016). <https://doi.org/10.1016/j.carbpol.2016.08.024>
 34. Yang, M., Zhang, Z.L., He, Y., Li, C.L., Wang, J.M., Ma, X.: Study on the structure characterization and moisturizing effect of *Tremella* polysaccharide fermented from GCMCC5.39. *Food Sci Human Wellness* **10**(4), 471–479 (2021). <https://doi.org/10.1016/j.fshw.2021.04.009>
 35. Zhan, Q.P., Wang, Q., Lin, R.G., He, P., Lai, F.R., Zhang, M.M., Wu, H.: Structural characterization and immunomodulatory activity of a novel acid polysaccharide isolated from the pulp of *Rosa laevigata* Michx fruit. *Int J Biol Macromol* **145**, 1080–1090 (2020). <https://doi.org/10.1016/j.ijbiomac.2019.09.201>
 36. Tang, Y., Zhu, Z.Y., Liu, Y., Sun, H.Q., Song, Q.Y., Zhang, Y.M.: The chemical structure and anti-aging bioactivity of an acid polysaccharide obtained from rose buds. *Food Funct* **9**(4), 2300–2312 (2018). <https://doi.org/10.1039/c8fo00206a>

37. Lin, Y.Y., Zeng, H.Y., Wang, K., Lin, H., Li, P.F., Huang, Y.X., Zhou, S.Y., Zhang, W., Chen, C., Fan, H.J.: Microwave-assisted aqueous two-phase extraction of diverse polysaccharides from *Lentinus edodes*: Process optimization, structure characterization and antioxidant activity. *Int J Biol Macromol* **136**, 305–315 (2019). <https://doi.org/10.1016/j.ijbiomac.2019.06.064>
38. Wu, Z., Li, H., Wang, Y.D., Yang, D.J., Tan, H.J., Zhan, Y., Yang, Y., Luo, Y., Chen, G.: Optimization extraction, structural features and antitumor activity of polysaccharides from *Z. jujuba* cv. *Ruoqiangzao* seeds. *Int J Biol Macromol* **135**, 1151–1161 (2019). <https://doi.org/10.1016/j.ijbiomac.2019.06.020>
39. Yu, S.S., Yu, J., Dong, X.D., Li, S., Liu, A.J.: Structural characteristics and anti-tumor/-oxidant activity in vitro of an acidic polysaccharide from *Gynostemma pentaphyllum*. *Int J Biol Macromol* **161**, 721–728 (2020). <https://doi.org/10.1016/j.ijbiomac.2020.05.274>
40. Zhang, Y., Zhou, T., Wang, H.J., Cui, Z., Cheng, F., Wang, K.P.: Structural characterization and in vitro antitumor activity of an acidic polysaccharide from *Angelica sinensis* (Oliv.) Diels. *Carbohydr Polym* **147**, 401–408 (2016). <https://doi.org/10.1016/j.carbpol.2016.04.002>
41. Hao, Y.L., Sun, H.Q., Zhang, X.J., Wu, L.R., Zhu, Z.Y.: A novel acid polysaccharide from fermented broth of *Pleurotus citrinopileatus*: Hypoglycemic activity in vitro and chemical structure. *J Mol Struct* **1220** (2020). <https://doi.org/10.1016/j.molstruc.2020.128717>
42. Chen, Y. J., Jiang, X., Xie, H. Q.: Structural characterization and antitumor activity of a polysaccharide from ramulus mori. *Carbohydr Polym* **190**, 232–239 (2018). <https://doi.org/10.1016/j.carbpol.2018.02.036>
43. Xia, Y.G., Liang, J., Yang, B.Y., Wang, Q.H., Kuang, H.X.: Structural studies of an arabinan from the stems of *Ephedra sinica* by methylation analysis and 1D and 2D NMR spectroscopy. *Carbohydr Polym* **121**, 449–456 (2015). <https://doi.org/10.1016/j.carbpol.2014.12.058>
44. Ogawa, K., Tsurugi, J., Watanabe, T.: Complex of gel-forming β -1,3-D-glucan with congored in alkaline solution. *Chem. Lett.* **1**(8), 689–692 (1972). <https://doi.org/10.1246/cl.1972.689>
45. Riemann, M., Andreas, N., Fedoseeva, M., Meier, E., Weih, D., Freytag, H., Schmidt-Ullrich, R., Klein, U., Wang, Z.Q., Weih, F.: Central immune tolerance depends on crosstalk between the classical and alternative NF-kappaB pathways in medullary thymic epithelial cells. *J Autoimmun* **81**, 56–67 (2017). <https://doi.org/10.1016/j.jaut.2017.03.007>
46. Yang, B., Xiao, B., Sun, T.Y.: Antitumor and immunomodulatory activity of *Astragalus membranaceus* polysaccharides in H22 tumor-bearing mice. *Int J Biol Macromol* **62**, 287–290 (2013). <https://doi.org/10.1016/j.ijbiomac.2013.09.016>
47. Li, C.W., Chen, T.T.: A novel hematoxylin and eosin stain assay for detection of the parasitic dinoflagellate *Amoebophrya*. *Harmful Algae* **62**, 30–36 (2017). <https://doi.org/10.1016/j.hal.2016.12.003>
48. Wang, K.L., Chu, D.X., Wu, J., Zhao, M.L., Zhang, M.M., Li, B.J., Du, W.J., Du, J.M., Guo, R.X.: WITHDRAWN: Cinobufagin induced cell apoptosis and protective autophagy through the ROS/ MAPK signaling pathway. *Life Sci* **116642** (2019). <https://doi.org/10.1016/j.lfs.2019.116642>
49. Nair, J.J., Staden, J.V.: Cell cycle modulatory effects of *Amaryllidaceae* alkaloids. *Life Sci* **213**, 94–101 (2018). <https://doi.org/10.1016/j.lfs.2018.08.073>
50. Lai, C.Y., Hung, J.T., Lin, H.H., Yu, A.L., Chen, S.H., Tsai, Y.C., Shao, L.E., Yang, W.B., Yu, J.: Immunomodulatory and adjuvant activities of a polysaccharide extract of *Ganoderma lucidum* in vivo and in vitro. *Vaccine* **28**(31), 4945–4954 (2010). <https://doi.org/10.1016/j.vaccine.2010.05.037>
51. Zhao, L.Y., Dong, Y.H., Chen, G.T., Hu, Q.H.: Extraction, purification, characterization and antitumor activity of polysaccharides from *Ganoderma lucidum*. *Carbohydr Polym* **80**(3), 783–789 (2010). <https://doi.org/10.1016/j.carbpol.2009.12.029>

Publisher's Note Springer Nature remains neutral with regard to jurisdictional claims in published maps and institutional affiliations.

Springer Nature or its licensor (e.g. a society or other partner) holds exclusive rights to this article under a publishing agreement with the author(s) or other rightsholder(s); author self-archiving of the accepted manuscript version of this article is solely governed by the terms of such publishing agreement and applicable law.